A Stable Adaptive Observer for Hard-Iron and Soft-Iron Bias Calibration and Compensation for Two-Axis Magnetometers: Theory and Experimental Evaluation

Andrew R. Spielvogel¹ and Louis L. Whitcomb¹

Abstract—This paper addresses the problem of on-line estimation and compensation of the hard-iron and soft-iron biases of a 2-axis magnetometer under dynamic motion, utilizing only biased measurements from a 2-axis magnetometer.

The proposed adaptive observer formulates the relation between the true magnetic field vector and the magnetometer measurements as an algebraic system where the unknown biases enter linearly. The observer is shown to be globally stable. When the magnetometer measurements are persistently exciting (PE), the system is shown to be globally asymptotically stable, and the biases are shown to converge to their true values. The estimated biases are used to provide a calibrated magnetic field direction vector which is utilized to estimate magnetic geodetic heading.

The adaptive observer is evaluated in a numerical simulation and a full-scale vehicle trial. For the proposed observer: (i) knowledge of the instrument attitude is not required for sensor bias estimation, (ii) zero a priori knowledge of the local magnetic field vector magnitude or vector direction is needed, (iii) the system is shown to be globally stable, (iv) the error system is shown to be globally asymptotically stable when the measured magnetometer signal is PE. (v) magnetometer hard-iron and soft-iron bias compensation is shown to dramatically improve dynamic heading estimation accuracy.

Index Terms—Calibration and Identification, Learning and Adaptive Systems

I. INTRODUCTION

Dynamic instrumentation and estimation of vehicle attitude, especially geodetic heading, is critical to the accurate navigation of land, sea, and air vehicles in dynamic motion. Many of these land and sea vehicles are passively stable in roll and pitch, and hence, experience relatively modest changes in roll and pitch during normal operation (e.g. surface vehicles, autonomous underwater vehicles (AUVs), and underwater ROVs). For this class of vehicles, it is possible to use 2-axis magnetometers for estimating the heading of the vehicle. However, the accurate magnetic heading estimation is

Manuscript received: September 10, 2019; Revised December 10, 2019; Accepted January 2, 2020.

This paper was recommended for publication by Editor Dezhen Song upon evaluation of the Associate Editor and Reviewers' comments. This study was supported by the National Science Foundation under NSF award OCE-1435818 and IIS-1909182.

¹ The authors are with the Department of Mechanical Engineering, Johns Hopkins University, Baltimore, MD, 21218. {aspielv1,llw}@jhu.edu

Digital Object Identifier (DOI): see top of this page.

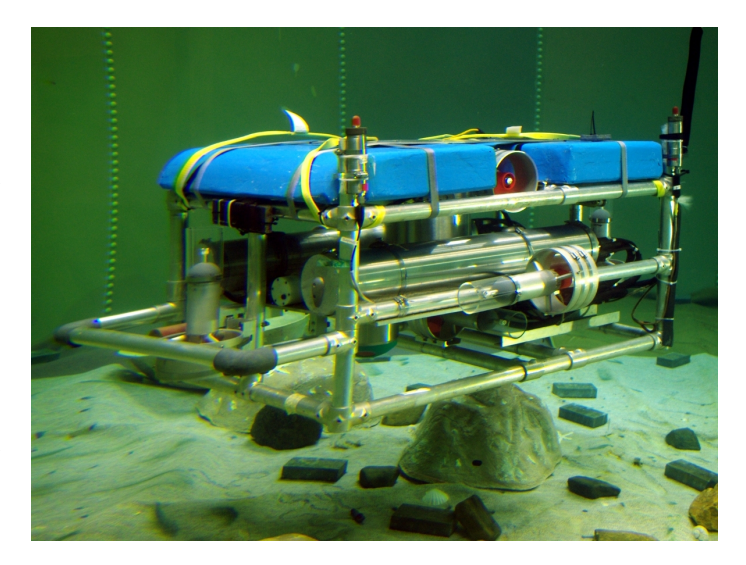


Fig. 1. The Full-scale experimental trial was conducted with the Johns Hopkins University (JHU) remotely operated vehicle (ROV) in a laboratory test tank (diameter of 7.5m and height of 4m). The JHU ROV has a full suite of navigation sensors, including several IMUs, typically found on deep submergence underwater vehicles.

commonly vitiated by very significant hard-iron and soft-iron magnetometer biases.

This paper reports a novel adaptive observer for real-time estimation of 2-axis magnetometer hard-iron and soft-iron iron biases of *dynamic* (rotating and translating) 2-axis magnetometers without *a priori* knowledge of the instrument's attitude or the instrument's local magnetic field vector. Unlike previous on-line approaches which utilize the extended Kalman filter (EKF), global stability of the error system is proved. Moreover, under a persistently exciting (PE) condition, the error system is shown to be globally asymptotic stable, and the sensor bias estimates are shown to converge to the true bias values. We report performance analyses in a numerical simulation study and in an actual full-scale experimental trial with a 2-axis magnetometer on the Johns Hopkins University (JHU) remotely operated vehicle (ROV) (Figure 1).

Advantages of the proposed approach include the following: (i) knowledge of the instrument attitude is not required for sensor bias estimation, (ii) zero a priori knowledge of the local magnetic field vector magnitude or vector direction is needed, (iii) the system is shown to be globally stable,

(iv) the error system is shown to be globally asymptotically stable when the measured magnetometer signal is PE. (v) magnetometer hard-iron and soft-iron bias compensation is shown to dramatically improve dynamic heading estimation accuracy.

A. Background and Motivation

Accurate sensing and estimation of heading is critical for precise navigation of a wide variety of vehicles. The need for accurate heading estimation is particularly acute in the case of vehicles operating in global positioning system (GPS)-denied environments such as underwater. Small low-cost underwater vehicles (UVs) commonly employ micro-electro-mechanical systems (MEMS) magnetometers to estimate local magnetic heading typically to within several degrees of accuracy, but require careful soft-iron bias and hard-iron bias calibration and compensation to achieve these accuracies. Moreover, magnetic heading sensors must be re-calibrated for soft-iron and hard-iron bias whenever the vehicle's physical configuration changes significantly (i.e. sensors or other payloads added or removed, etc.), as very frequently occurs on oceanographic marine vehicles. Studies have shown that the accuracy of these magnetic heading sensors can be a principal error source in overall navigation solutions [12]. Thus, when employing magnetic heading sensors it is essential to accurately estimate sensor biases in order to achieve high accuracy heading estimation.

In the design of surface and underwater oceanographic vehicles, great care is taken to isolate and separate on-board magnetic compasses from any possible time-varying on-board magnetic disturbance sources. Active electro-magnetic components are chosen to have closed magnetic flux-paths, and magnetic compass heading are located as far as possible from on-board passive magnetic, passive permeable, and active electro-magnetic components. With proper design, time-varying on-board magnetic disturbance can be rendered negligible. What remains an ubiquitous problem, however, and is the focus of this paper, is the estimation and compensation for the the effects of the magnetic bias ("hard iron") and permeability ("soft iron") of the entire vehicle on the compass heading.

B. Literature Review

Several methods for magnetometer bias estimation have been reported in recent years. Alonso and Shuster proposed the "TWOSTEP" method [1] for estimating magnetometer hardiron sensor bias, and in later work, an extended method for calibrating magnetometer scale and orthogonality factors, or soft-iron bias, as well [2]. Vasconselos et al. present bias estimation (hard-iron and soft-iron) as an ellipsoid fitting problem which can be solved with an iterative maximum likelihood estimate (MLE) approach [27]. Many least squares methods are reported for the ellipsoid fitting problem (e.g. [3], [5], [6], [18]) and Wu et al. [29] frame the ellipsoid fitting problem as a particle swarm optimization (PSO). Kok et al. [13] and Li and Li [15] fuse accelerometer measurements with magnetometer measurements to estimate magnetometer sensor bias, and Papafotis and Sotiriadis [19] report an algorithm for

three-axis accelerometer and magnetomoter calibration using a gradient decent method. These methods, however, are batch estimators that are not practical for on-line estimation of magnetometer sensor bias.

Sensor biases change over time due to changes in sensor payload, temperature, local field disturbances, etc., which make it imperative to estimate sensor biases in real time. In ([23], [26]) the authors report adaptive methods utilizing magnetometer and gyroscope measurements for estimating 3-axis magnetometer hard-iron sensor biases, but these approaches do not address soft-iron bias estimation.

Crassidis et al. report an extension to the TWOSTEP method based on the EKF [4] and Guo et al. present an alternative EKF approach for doing magnetometer sensor bias estimation [7]. Han et al. [9] report a gyroscope-aided EKF method for magnetic calibration. However, these studies do not report analytical guarantees of the stability or the convergence of the sensor biases to their true values.

Soken and Sakai [22] report a magnetometer calibration method using the TRIAD algorithm and an unscented Kalman filter (UKF). However, this method requires knowledge of the initial attitude of the instrument, has a slow convergence time, and the study reports no stability guarantees.

The present paper reports a novel method for real-time softiron and hard-iron bias calibration for 2-axis magnetometers utilizing only biased measurements from a 2-axis magnetometer. The proposed algorithm is shown to be globally asymptotically stable when the measured magnetometer is PE, does not require local field information for calibrating the measured magnetic field vector direction, does not require any knowledge of the instrument's attitude, and can easily be implemented on-line in real-time.

C. Paper Outline

This paper is organized as follows: Section II gives an overview of the magnetometer measurement model. Section III reports the adaptive soft and hard iron observer and Section IV reports a least squares approach. Section V presents numerical simulation evaluation of the observer. Section VI reports a full scale vehicle trial. Section VII summarizes and concludes.

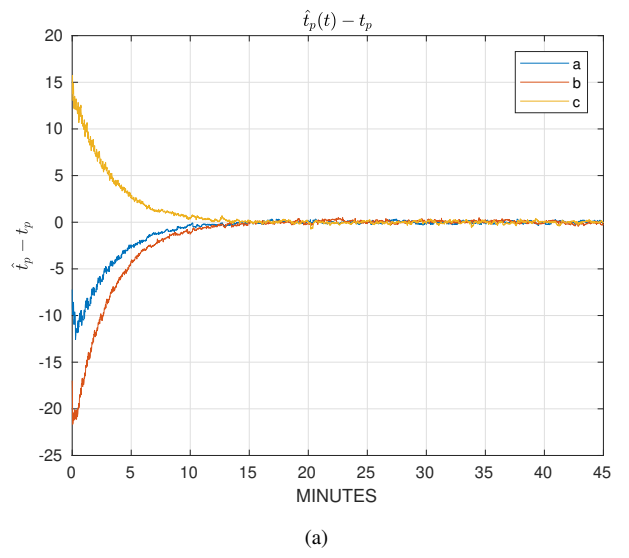
II. MAGNETOMETER MEASUREMENT MODEL

Magnetometers (including those employed in IMUs) are subject to two primary sensor calibration errors: hard-iron and soft-iron. Hard-iron errors are constant magnetometer sensor bias terms due to the permanent magnetic signature of the instrument and the vehicle. Soft-iron errors are non-constant magnetometer sensor bias terms due to the magnetic permeability of the instrument and the vehicle, and will vary with vehicle heading and attitude. For most IMU magnetometers, hard-iron errors dominate soft-iron errors.

We define the following measurement model for 2-axis magnetometers:

$$m_m(t) = Tm_t(t) + b (1)$$

where $m_m(t) \in \mathbb{R}^2$ is the noise-free magnetometer measurement, $m_t(t) \in \mathbb{R}^2$ is Earth's true magnetic field, $T \in \mathbb{R}^{2 \times 2}$



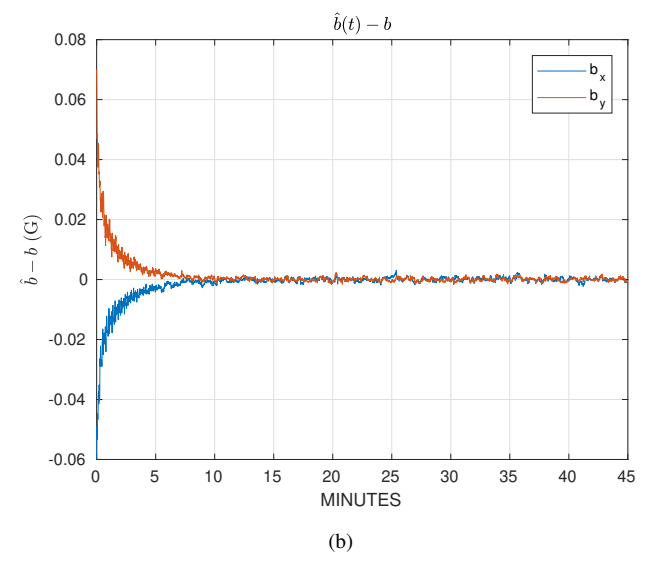


Fig. 2. Simulation: (a) The parameter error of the estimated $\hat{t}_p(t)$ from the true value t_p . a, b, c are the components of t_p as defined in (15). (b) The parameter error of the estimated $\ddot{b}(t)$ from the true value b where b_x, b_y are the x and y components of the hard-iron sensor bias.

is a diagonally-dominant positive definite symmetric (PDS) matrix representing soft-iron bias, and $b \in \mathbb{R}^2$ represents the magnetometer hard-iron bias.

III. ADAPTIVE SOFT-IRON AND HARD-IRON BIAS **OBSERVER**

This section reports the derivation of a novel on-line adaptive observer for hard-iron and soft-iron magnetometer biases in 2-axis magnetometers. The biases are assumed to be very slowly time varying, and hence we model them as constant terms and update the estimates continuously.

A. Magnetometer Bias System Model

We can rearrange (1) as

$$m_t(t) = T^{-1} (m_m(t) - b).$$
 (2)

Taking the inner product of (2) with itself results in

$$||m_t(t)||^2 = (m_m(t) - b)^T T^{-2} (m_m(t) - b)$$

$$= m_m^T(t) T^{-2} m_m(t) - 2m_m^T(t) T^{-2} b + b^T T^{-2} b.$$
(4)

Subtracting $b^T T^{-2} b$ from both sides results in

$$\phi = m_m^T(t)T^{-2}m_m(t) - 2m_m^T(t)T^{-2}b \tag{5}$$

where $\phi = ||m_t(t)||^2 - b^T T^{-2} b$. Dividing both sides of (5) by ϕ results in

$$1 = m_m^T(t)\Gamma m_m(t) - 2m_m^T \alpha \tag{6}$$

where $\Gamma \in \mathbb{R}^{2 \times 2}$ and $\alpha \in \mathbb{R}^2$ are defined as

$$\Gamma = T^{-2}/\phi \tag{7}$$

and

$$\alpha = T^{-2}b/\phi. \tag{8}$$

We note that this approach only works when ϕ is not close to zero. Thus, we require that the hard-iron bias is smaller than the magnitude of the true magnetic field vector. Fortunately, this condition is true for most magnetometers.

Using the identity

$$\operatorname{vec}(AXB) = (B^T \otimes A)\operatorname{vec}(X) \tag{9}$$

(6) can be written as

$$1 = \begin{bmatrix} m_m^T(t) \otimes m_m^T(t) & -2m_m^T(t) \end{bmatrix} \begin{bmatrix} \operatorname{vec}(\Gamma) \\ \alpha \end{bmatrix}$$
 (10)

where \otimes is the Kronecker product and vec (\cdot) is the vectorization (or "stack") operator [21].

Using the common assumption that the soft-iron bias term T is a PDS matrix, Γ is parameterized as

$$\Gamma = \left[\begin{array}{cc} a & c \\ c & b \end{array} \right]. \tag{11}$$

Using this parameterization and rearranging terms in (10), the system model becomes

$$1 = w^T(t)\theta \tag{12}$$

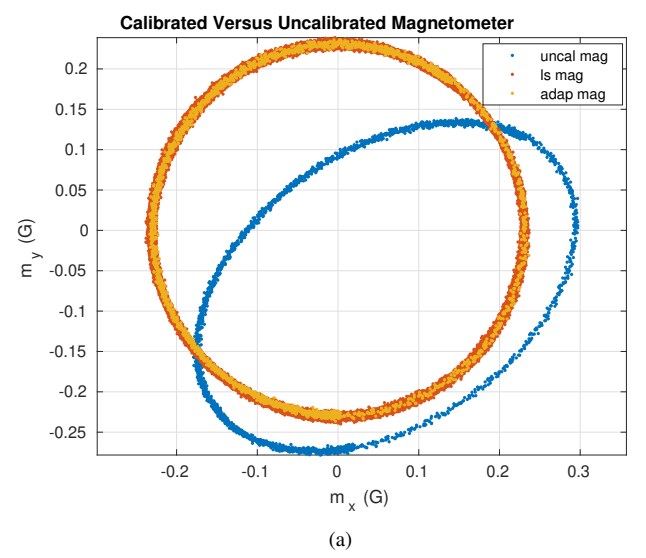
where

$$w(t) = \begin{bmatrix} m_x^2(t) \\ m_y^2(t) \\ 2m_x(t)m_y(t) \\ -2m_m(t) \end{bmatrix},$$
(13)
$$\theta = \begin{bmatrix} t_p \\ \alpha \end{bmatrix},$$
(14)

$$\theta = \begin{bmatrix} t_p \\ \alpha \end{bmatrix}, \tag{14}$$

$$t_p = \begin{bmatrix} a \\ b \\ c \end{bmatrix}, \tag{15}$$

where $m_x(t) \in \mathbb{R}$ and $m_y(t) \in \mathbb{R}$ are the x and y components of magnetometer measurement signal $m_m(t)$ respectively, $w(t) \in \mathbb{R}^5$ is a known nonlinear time-varying function of the measured magnetometer signal $m_m(t)$, and $\theta \in \mathbb{R}^5$ is a



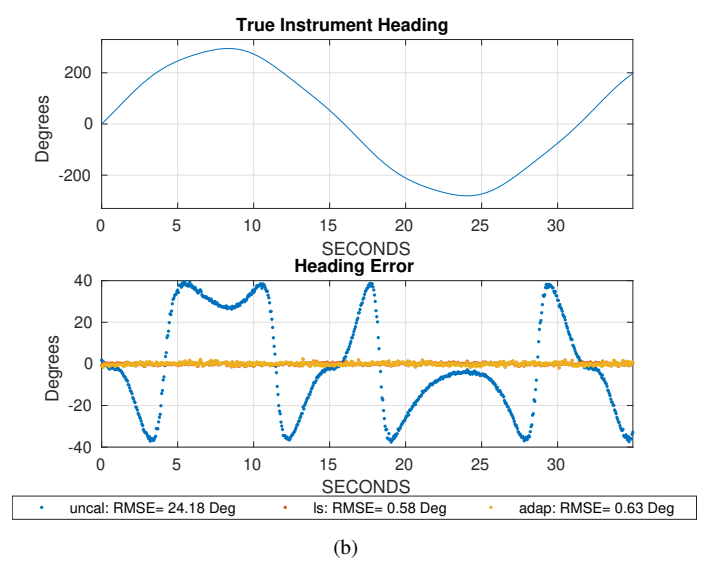


Fig. 3. **Simulation:** (a) Comparison of the uncalibrated (uncal), least squares (ls) calibrated, and adaptive observer (adap) calibrated magnetometer measurements. (b) *Top:* The true instrument heading from the first 35 seconds of the simulation. *Bottom:* Heading error corresponding to the uncalibrated (uncal), least squares (ls) calibrated, and adaptive observer (adap) calibrated magnetometers during the first 40 seconds of the simulation.

constant vector encoding the true soft-iron and hard-iron bias parameters.

B. Adaptive Observer for Hard-Iron and Soft-Iron Bias

We note that the algebraic system (12) has the same form as the vector input, single output system presented in Chapter 3 of [16]. (12) can be rearranged such that the exact true plant takes the form

$$0 = w^T(t)\theta - 1. (16)$$

Defining $\hat{\theta}(t)$ as the adaptive identifier's estimate of the (unknown) true parameter θ , the identifier plant takes the form

$$e(t) = w^{T}(t)\hat{\theta}(t) - 1 \tag{17}$$

$$= w^{T}(t)\Delta\theta \tag{18}$$

where e(t) as the error associated with the identifier plant, and $\Delta\theta(t)$ is the parameter error

$$\Delta\theta(t) = \hat{\theta}(t) - \theta. \tag{19}$$

Note that since θ is constant

$$\Delta \dot{\theta}(t) = \dot{\hat{\theta}}(t). \tag{20}$$

The adaptive observer's parameter update law for the parameter $\hat{\theta}(t)$ is chosen to be

$$\Delta \dot{\theta}(t) = -Kw(t)e(t) \tag{21}$$

$$\dot{\hat{\theta}}(t) = -Kw(t)w^{T}(t)\hat{\theta}(t) + Kw(t) \tag{22}$$

where $K \in \mathbb{R}^{5 \times 5}$ is a constant PDS adaptation gain matrix.

C. Stability Analysis

Consider the Lyapunov function candidate

$$V = \frac{1}{2} \Delta \theta^{T}(t) K^{-1} \Delta \theta(t). \tag{23}$$

where V is a positive definite, C^1 , and radially unbounded function by construction. The time derivative of (23) is

$$\dot{V} = \Delta \theta^T(t) K^{-1} \Delta \dot{\theta}(t) \tag{24}$$

$$= -\Delta \theta^{T}(t)w(t)e(t) \tag{25}$$

$$= -\Delta \theta^{T}(t)w(t)w^{T}(t)\Delta \theta(t)$$
 (26)

$$< 0.$$
 (27)

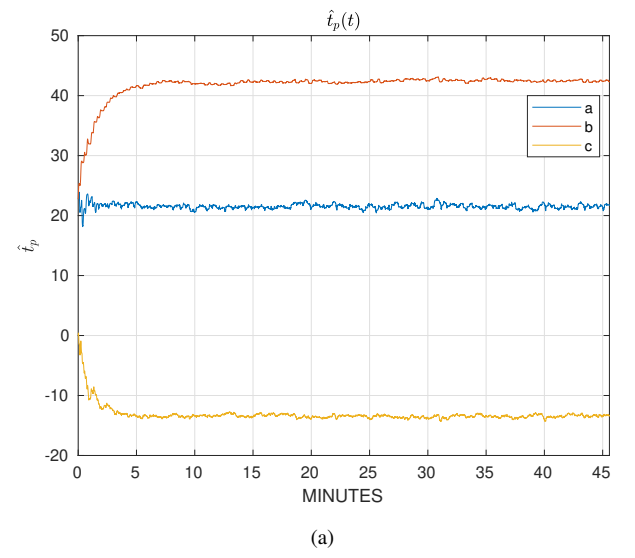
Thus \dot{V} is negative semi-definite, and the error system (21) is globally stable. If, in addition, w(t) is PE ([16], [20]), the error system is globally asymptotically stable. That is, if there exists finite $\alpha, \beta, T > 0$ such that

$$\alpha I \le \int_{t}^{t+T} w(\tau) w^{T}(\tau) d\tau \le \beta I$$
 (28)

for all $t\geq 0$ and I is the identity matrix, then the proposed observer is globally asymptotically stable and $\lim_{t\to\infty}\hat{\theta}(t)=\theta$. It is unclear how to show analytically that a PE $m_m(t)$ signal implies that w(t) is PE. We were able to check numerically, however, that a variety of PE $m_m(t)$ signals all resulted in a PE w(t), thus satisfying the conditions of (28). Moreover, the resulting numerically simulated system was observed to be asymptotically stable.

IV. LEAST SQUARES SOFT-IRON AND HARD-IRON ESTIMATION

This section reports the derivation of a least squares approach for hard-iron and soft-iron magnetometer biases in 2-axis magnetometers to be used as a comparison to the adaptive observer presented in the previous section. As in the previous section, the biases modeled as constant terms.



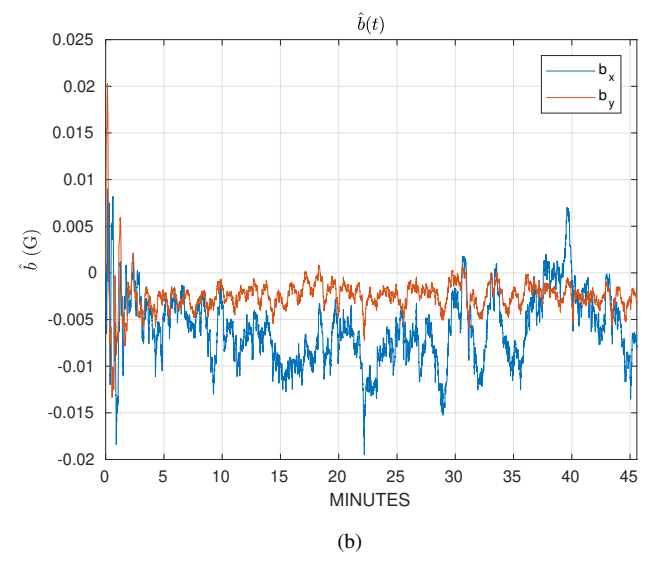


Fig. 4. Vehicle Trial Experiment: (a) The adaptive observer's estimated $\hat{t}_p(t)$ where a, b, c are the components of t_p as defined in (15). (b) The adaptive observer's estimated $\hat{b}(t)$ where b_x, b_y are the x and y components of the hard-iron sensor bias.

From (12), the i^{th} measurement satisfies

$$1 = w_i^T(t)\theta \tag{29}$$

where

$$w_{i}(t) = \begin{bmatrix} m_{x,i}^{2}(t) \\ m_{y,i}^{2}(t) \\ 2m_{x,i}(t)m_{y,i}(t) \\ -2m_{m,i}(t) \end{bmatrix},$$
(30)

 $m_{m,i}(t)$ is the i^{th} magnetometer measurement and $m_{x,i}(t)$, $m_{y,i}(t)$ are the x and y components of $m_{m,i}(t)$ respectively. By arranging the w_i vectors such that

$$W^{T} = \begin{bmatrix} w_1^T \\ w_2^T \\ \vdots \\ w_n^T \end{bmatrix}$$
 (31)

(29) can be rewritten as

$$\begin{bmatrix} 1\\1\\\vdots\\1 \end{bmatrix} = \begin{bmatrix} w_1^T\\w_2^T\\\vdots\\w_n^T \end{bmatrix} \theta$$

$$= W^T \theta.$$
(32)

The least squares solution θ^* is then found by Moore-Penrose inverse

$$\theta^* = \left(WW^T\right)^{-1}W\begin{bmatrix} 1\\1\\\vdots\\1 \end{bmatrix}. \tag{34}$$

V. NUMERICAL SIMULATION EVALUATION

The instantaneous estimated heading can then be computed as

$$\hat{\gamma} = atan2 (-m_y, m_x) - \gamma_0, [25]$$
 (35)

where γ_0 is the known local magnetic variation and where $m_x \in \mathbb{R}$, $m_y \in \mathbb{R}$ are the x and y components, respectively, of the m_m signal.

A. Simulation Setup

The magnetometer sensor bias observer is evaluated in a numerical simulation.

- Sensor measurements were simulated to represent the magnetometer of the KVH 1775 IMU (KVH Industries, Inc., Middletown, RI, USA) [14].
- Magnetometer sensor measurement sampling was simulated at 20 Hz.
- Simulated magnetometer measurements include sensor noise of $\sigma_m=0.002$ Gauss (G) which is consistent with the KVH 1775 IMU.
- The simulated hard-iron magnetometer measurement bias

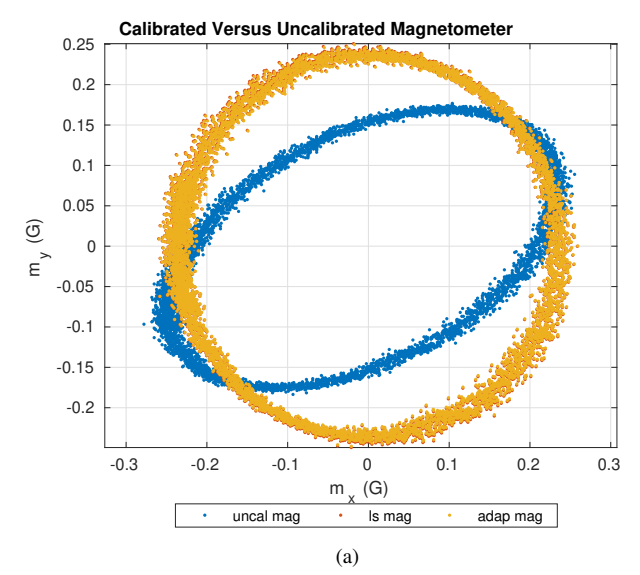
$$b = \begin{bmatrix} 0.06 \\ -0.07 \end{bmatrix} G \tag{36}$$

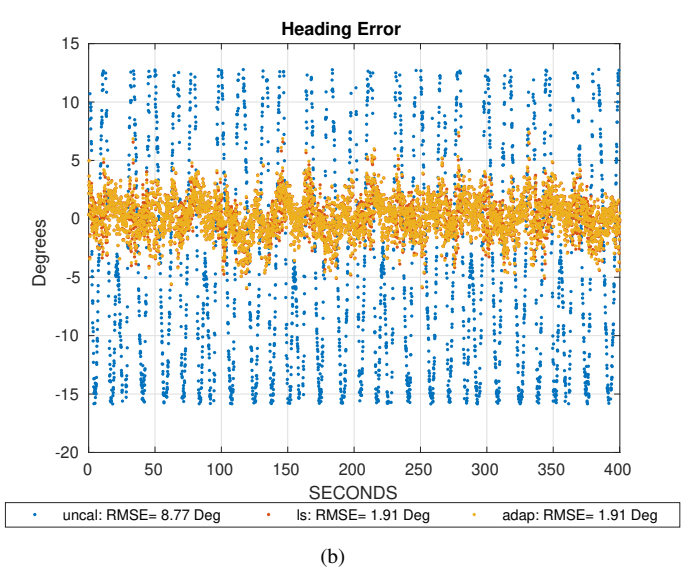
which is consistent with hard-iron biases observed experimentally with the KVH 1775 IMU.

The simulated soft-iron magnetometer measurement bias

$$T = \begin{bmatrix} 1.1 & 0.2 \\ 0.2 & 0.95 \end{bmatrix}. \tag{37}$$

- Simulations were for a latitude of $39.32^{\circ}N$ and a longitude of 76.62W.
- The simulated instrument was commanded to execute smooth sinusoidal rotations of roughly ±300° in heading.





Vehicle Trial Experiment: (a) Comparison of the uncalibrated (uncal), least squares (ls) calibrated, and adaptive observer (adap) calibrated magnetometer measurements. (b) Heading error corresponding to the uncalibrated (uncal), least squares (ls) calibrated, and adaptive observer (adap) calibrated magnetometers during the first 400 seconds of the vehicle trial experiment.

· The observer's initial conditions were set to

$$\hat{\theta}(t) = \begin{bmatrix} 1 & 1 & 0 & 0 & 0 \end{bmatrix}^T / \phi \tag{38}$$

where

$$\phi = \|m_t\|^2 \tag{39}$$

$$= \| \begin{bmatrix} 0.205796 & -0.040654 \end{bmatrix} \|^2 G.$$
 (40)

• The gain matrix used during the simulation was

$$K = diag([100 \ 100 \ 100 \ 1 \ 1]).$$
 (41)

B. Simulation Results

The parameter errors from the simulation are shown in Figure 2 where the recovered value for the estimated hardiron bias term $\hat{b}(t)$ is found by

$$\hat{b}(t) = \hat{\Gamma}^{-1}(t)\hat{\alpha}(t). \tag{42}$$

The simulation results show that when the magnetometer measurements are PE, the parameter estimates converge to their true values.

Note that Γ is T^{-2} scaled by $1/\phi$. Therefore, in order to recover the true soft-iron bias, T, knowledge of the true magnetic field magnitude is necessary. However, since the calibrated magnetometer measurement is commonly used as a reference direction in attitude and heading reference systems (AHRSs) ([8], [28]), recovering the true magnitude of T is **not** critical to the accurate estimation of heading. However, if $||m_t(t)||$ is known (For field vehicles, the local magnetic field strength is commonly estimated by magnetic field models like the World Magnetic Model (WMM) [17] or the International Geomagnetic Reference Field (IGRF) model [24].), ϕ can be recovered by

$$\phi = ||m_t||^2 - b^T T^{-2} b \tag{43}$$

$$= \|m_t\|^2 - \phi b^T \Gamma b \tag{44}$$

$$= ||m_t||^2 - \phi b^T \Gamma b$$

$$= \frac{||m_t||^2}{1 + b^T \Gamma b}$$
(44)

and hence, the true T can be recovered.

Using the simulation's final parameter estimates, $\hat{\Gamma}(t_f)$ and $\hat{b}(t_f)$ to calibrate the magnetometer, the heading estimate of the instrument is calculated by (35). Figure 3 shows the comparison between the uncalibrated and calibrated magnetometer measurements and the corresponding heading and heading error of the instrument during part of the simulated experiment. The simulation shows that after the sensor bias estimates have converged, the calibrated magnetometer corresponds to a heading root mean square error (RMSE) of 0.63°. This is a vast improvement over the heading RMSE 24.2° corresponding to the uncalibrated magnetometer and very close to the error corresponding to the least squares calibrated magnetometer of 0.58° .

VI. VEHICLE TRIAL EVALUATION

A. Experimental Test Facility

Experimental trials were performed with the JHU remotely operated vehicle (ROV), equipped with a KVH 1775 IMU (KVH Industries, Inc., Middletown, RI, USA) [14], in the 7.5 m diameter, 4 m deep fresh water test tank in the JHU hydrodynamic test facility (HTF). The ROV is a fully actuated (six-degrees of freedom (DOF)) vehicle with six 1.5 kW DC brushless electric thrusters and employs a suite of sensors commonly employed on deep submergence underwater vehicles. This includes a high-end inertial navigation system (INS), the iXBlue PHINS III (iXBlue SAS, Cedex, France) ([10], [11]), that is used as a "ground-truth" comparison during the experimental trials. The PHINS is a high-end

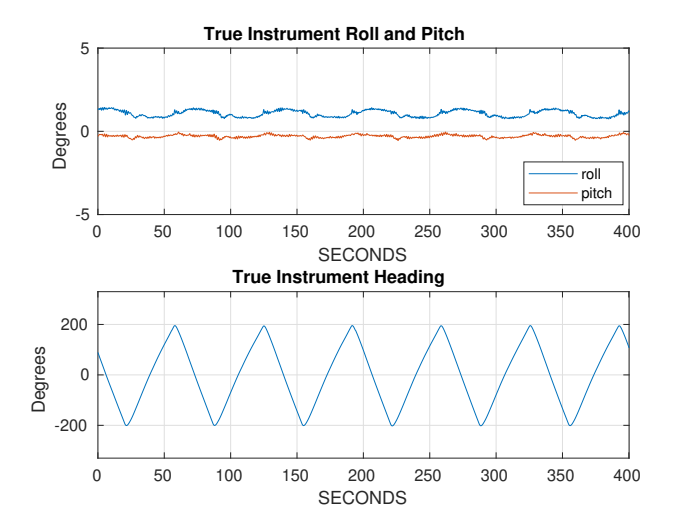


Fig. 6. True instrument heading, pitch, and roll from the first 400 seconds of the vehicle trial experiment.

INS (\sim \$120k) with roll, pitch, heading accuracies of 0.01° , 0.01° , 0.05° / $\cos(\text{latitude})$, respectively ([10]). Figure 1 shows the JHU-ROV operating in the test tank. The JHU ROV is passively stable in roll and pitch due to a large center-of-gravity to center-of-buoyancy separation, and experiences limited roll and pitch excursions in normal operation.

B. Experimental Setup

The adaptive observer for hard-iron and soft-iron magnetometer sensor biases is evaluated with a full scale vehicle trial employing the MEMS magnetometer in the KVH 1775 IMU.

- The magnetometer was sampled at 20 Hz.
- The magnetometer was aligned via a fixture to the ROV's iXBLUE PHINS INS (iXblue SAS, Cedex, France).
 The PHINS attitude is used as ground truth during the experimental evaluation of the observer.
- The experiment was conducted at a latitude of 39.32°N and a longitude of 76.62W.
- The JHU ROV was commanded to execute smooth sinusoidal rotations of roughly $\pm 200^\circ$ in heading while in closed loop control.
- The initial conditions for the sensor bias estimates are given by (38)-(40).
- The gain matrix K used during the vehicle trial was (41), the same as in the simulation evaluation.

C. Experimental Results

The estimated parameters from the experiment are shown in Figure 4 where the estimated hard iron bias term $\hat{b}(t)$ is calculated by (42). The vehicle trial results show that when the magnetometer measurements are PE, the parameter estimates converge to a steady-state value.

In experimental trials, the true sensor biases are unknown, and thus the accuracy of the estimated biases cannot be measured directly. Instead, the accuracy of the heading estimate is used as an error metric for sensor bias estimation.

As discussed in Section V-B, $\hat{t}_p(t)$ and $\hat{b}(t)$ can be used to calibrate the magnetometer measurements for a calibrated magnetic field reference direction that is used for heading estimation in AHRSs.

Figure 5 shows the comparison between the uncalibrated, least squares calibrated, and adaptive observer calibrated magnetometer measurements and the corresponding heading error of the instrument during part of the vehicle trial. The experiment shows that the adaptive observer calibrated magnetometer corresponds to a heading RMSE of 1.91°, which is identical to the heading RMSE corresponding to the least squares calibrated magnetometer and much improved over the heading RMSE of 8.77° of the uncalibrated magnetometer.

Figure 6 shows the true roll, pitch, and heading of the vehicle during the first 400 seconds of vehicle trial. The vehicle experienced very limited roll and pitch excursions during the vehicle trial.

Note that, in this experimental trial, the parameter initial condition was chosen to be far from the true parameter. Because of this, the estimated parameter had to evolve far from the initial condition to the true parameter. Hence, the gain matrix K was chosen to be large to facilitate fast convergence of the parameter. In the presence of measurement noise, smaller gains allow the estimated parameter to converge to a smaller neighborhood of the true parameter than higher gains. However, this increase in accuracy comes with a longer convergence time. The gain matrix K, used in the experimental evaluation, provided a balance of accuracy and fast convergence. It is important to note that in adaptive systems there is no method for choosing "ideal" gains. Instead the gain matrix K must be tuned empirically. The sensor noise, the amount of PE the instrument experiences, and the accuracy of the initial guess of the bias terms all affect the rate of convergence and the size of the neighborhood that the estimated parameters converge to. When tuning K, the diagonal gains should be chosen large enough such that the parameters converge to a steady-state neighborhood while small enough that the parameters do not oscillate. This is a balancing act as the higher the gains, the faster the parameters will converge to a neighborhood of the true parameters but the neighborhood will be larger. Similarly, the smaller the gains, the slower the convergence, but the neighborhood will be smaller.

In practice, after an initial calibration of the magnetometer, the previous parameter estimate could be used as an initial condition. Thus, after a rough alignment, a smaller gain matrix can be chosen to provide a more accurate estimate of the true parameter.

VII. CONCLUSION

This paper reports a novel adaptive observer for on-line, real-time estimation of hard-iron and soft-iron magnetometer biases in 2-axis magnetometers for use in AHRSs. AHRSs commonly use calibrated magnetometers as a measurement of the magnetic field direction for estimating heading. The accuracy of these systems rely on the calibrated magnetometer direction to be accurate, but do not require the correct

magnitude of the calibrated magnetometer. Estimating the magnetometer's soft-iron bias up to a scale factor preserves the calibrated magnetometer's direction. Hence, the proposed approach which observes a scaled version of T, can be utilized to bias-compensate magnetometers to provide accurate heading estimates.

The observer uses only magnetometer sensor signals, does not require knowledge of the instrument attitude, and is shown to be globally stable. When the measured magnetometer is PE, the observer is shown to be globally asymptotically stable where the estimated parameters converge to their true values. The simulation study and full-scale vehicle experiment suggest that the observer can be utilized to provide accurate magnetometer bias compensation for AHRS. The vehicle trial shows that the estimated parameters converge to a steady state and the calibrated magnetometer's corresponding heading estimate tracks ground truth heading to 1.9° RMSE which is the RMSE corresponding to the least squares calibration.

In future studies, the authors hope to develop a coarse and fine alignment protocol to allow for fast convergence and accurate bias estimation and employ the observer in field trials.

REFERENCES

- R. Alonso and M. D. Shuster. TWOSTEP: A fast robust algorithm for attitude-independent magnetometer-bias determination. *Journal of the Astronautical Sciences*, 50(4):433–452, 2002.
- [2] R. Alonso and M. D. Shuster. Complete linear attitude-independent magnetometer calibration. *Journal of the Astronautical Sciences*, 50(4):477–490, 2002.
- [3] N. Ammann, A. Derksen, and C. Heck. A novel magnetometeraccelerometer calibration based on a least squares approach. In 2015 International Conference on Unmanned Aircraft Systems (ICUAS), pages 577–585, June 2015.
- [4] J. L. Crassidis, K.-L. Lai, and R. R. Harman. Real-time attitudeindependent three-axis magnetometer calibration. *Journal of Guidance*, *Control, and Dynamics*, 28(1):115–120, 2005.
- [5] J. Fang, H. Sun, J. Cao, X. Zhang, and Y. Tao. A novel calibration method of magnetic compass based on ellipsoid fitting. *IEEE Trans*actions on Instrumentation and Measurement, 60(6):2053–2061, June 2011
- [6] C. C. Foster and G. H. Elkaim. Extension of a two-step calibration methodology to include nonorthogonal sensor axes. *IEEE Transactions* on Aerospace and Electronic Systems, 44(3):1070–1078, July 2008.
- [7] P. Guo, H. Qiu, Y. Yang, and Z. Ren. The soft iron and hard iron calibration method using extended Kalman filter for attitude and heading reference system. In *Position, Location and Navigation Symposium*, 2008 IEEE/ION, pages 1167–1174. IEEE, 2008.
- [8] T. Hamel and R. Mahony. Attitude estimation on SO(3) based on direct inertial measurements. In 2006 IEEE International Conference on Robotics and Automation (ICRA), pages 2170–2175. IEEE, 2006.
- [9] K. Han, H. Han, Z. Wang, and F. Xu. Extended Kalman filter-based gyroscope-aided magnetometer calibration for consumer electronic devices. *IEEE Sensors Journal*, 17(1):63–71, Jan 2017.

- [10] iXblue SAS, Cedex, France. iXSEA PHINS INS datasheet, 2008.
- [11] IXSEA. PHINS III User Guide. IXSEA, MU-PHINSIII-006 B edition, December 2008.
- [12] J. C. Kinsey and L. L. Whitcomb. Preliminary field experience with the DVLNAV integrated navigation system for oceanographic submersibles. *Control Engineering Practice*, 12(12):1541 – 1549, 2004. Guidance and control of underwater vehicles.
- [13] M. Kok, J. D. Hol, T. B. Schön, F. Gustafsson, and H. Luinge. Calibration of a magnetometer in combination with inertial sensors. In *Information Fusion (FUSION)*, 2012 15th International Conference on, pages 787–793. IEEE, 2012.
- [14] KVH Industries, Inc., Middletown, RI, USA. KVH 1775 IMU datasheet, 2019.
- [15] X. Li and Z. Li. A new calibration method for tri-axial field sensors in strap-down navigation systems. *Measurement Science and technology*, 23(10):105105, 2012.
- [16] K. S. Narendra and A. M. Annaswamy. Stable adaptive systems. Prentice-Hall Inc., 1989.
- [17] NCEI Geomagnetic Modeling Team and British Geological Survey. World Magnetic Model 2020. National Centers for Environmental Information, 2019.
- [18] H. S. Ousaloo, G. Sharifi, J. Mahdian, and M. T. Nodeh. Complete calibration of three-axis strapdown magnetometer in mounting frame. *IEEE Sensors Journal*, 17(23):7886–7893, Dec 2017.
- [19] K. Papafotis and P. P. Sotiriadis. Computationally efficient calibration algorithm for three-axis accelerometer and magnetometer. In 2019 8th International Conference on Modern Circuits and Systems Technologies (MOCAST), pages 1–4, May 2019.
- [20] S. Sastry and M. Bodson. Adaptive control: stability, convergence and robustness. Prentice-Hall Inc., 1989.
- [21] Schäcke, Kathrin. On the Kronecker Product. Master's thesis, University of Waterloo, 2013.
- [22] H. E. Soken and S. Sakai. Triad+filtering approach for complete magnetometer calibration. In 2019 9th International Conference on Recent Advances in Space Technologies (RAST), pages 703–708, June 2019.
- [23] A. R. Spielvogel and L. L. Whitcomb. Adaptive Sensor Bias Estimation in Nine Degree of Freedom Inertial Measurement Units: Theory and Preliminary Evaluation. In 2018 IEEE/RSJ International Conference on Intelligent Robots and Systems (IROS), pages 5555–5561, Oct 2018.
- [24] E. Thébault, C. C. Finlay, et al. International Geomagnetic Reference Field: the 12th generation. Earth, Planets, and Space, 67:79, May 2015.
- [25] G. Troni. Advances in precision navigation of underwater vehicles. PhD thesis, Johns Hopkins University, 2013.
- [26] G. Troni and L. L. Whitcomb. Field sensor bias calibration with angularrate sensors: Theory and experimental evaluation with application to magnetometer calibration. *IEEE/ASME Transactions on Mechatronics*, 24(4):1698–1710, Aug 2019.
- [27] J. F. Vasconcelos, G. Elkaim, C. Silvestre, P. Oliveira, and B. Cardeira. Geometric Approach to Strapdown Magnetometer Calibration in Sensor Frame. *IEEE Transactions on Aerospace and Electronic Systems*, 47(2):1293–1306, April 2011.
- [28] T. H. Wu, E. Kaufman, and T. Lee. Globally Asymptotically Stable Attitude Observer on SO(3). In 2015 54th IEEE Conference on Decision and Control (CDC), pages 2164–2168, Dec 2015.
- [29] Z. Wu, Y. Wu, X. Hu, and M. Wu. Calibration of three-axis magnetometer using stretching particle swarm optimization algorithm. *IEEE Transactions on Instrumentation and Measurement*, 62(2):281–292, Feb 2013.